ADVANCED MATERIALS
www.advmat.de

Highly Sensitive Photoelectric Detection and Imaging Enhanced by the Pyro-Phototronic Effect Based on a Photoinduced Dynamic Schottky Effect in 4H-SiC

Yueming Zhang, Yi-Chi Wang, Longfei Wang, Laipan Zhu, and Zhong Lin Wang**

Silicon carbide (SiC), one of the third-generation semiconductor materials with excellent electrical and optoelectronic properties, is ideal for high light-sensing performance. Here, a self-powered SiC ultraviolet (UV) photodetector (PD) is constructed with wider applicability and higher commercialization potential. The great performance of the PD is realized by a remarkable photoinduced dynamic Schottky effect derived from the symbiotic modulation of Schottky and Ohmic contact. Using the pyro-phototronic effect that exists in the N-doped 4H-SiC single crystal PDs, a fast pyroelectric response time of 0.27 s is achieved, which is almost ten times shorter than that obtained from the steady-state signal under UV illumination. The maximal transient photoresponsivity reaches 9.12 nA mW^{-1}, which is ≈20% higher than the conventional photoelectric signal. Moreover, different regions of the 4H-SiC centimeter-scale chip output distinct signals under UV illumination, demonstrating efficient optical imaging and information transmission capabilities of this device. This work not only reveals the fundamental optoelectronic physics lying in this vital third-generation semiconductor, but also sheds light on its potential photosensing applications for large-scale commercialization.

1. Introduction

As a third-generation semiconductor, silicon carbide (SiC) has become a strategic material for power electronics because of its high efficiency,[1] high electron saturation drift speed,[2] and excellent thermal conductivity and stability[3] for photoelectric detection.[4] Although various SiC-based photodetectors (PDs) exist,[5] most of them have certain limitations, including complex fabrication process, prohibitive cost, structural complexity, and single function for just light intensity sensing. It would be much desired if more efficient and diverse information transmission can be achieved in such SiC PDs.[6] Moreover, ordinary planar PDs always require an external power supply. The breakthrough of self-powered supply by utilizing the properties of the semiconductor itself provides a new approach for its independent and sustainable operation. In this way, the photoelectric detector could be driven by the signal itself rather than external power sources or traditional batteries,[7] not only simplifying the circuit design but also ensuring the sustainable and stable use of the device in practice.

A single device with multifunction is often desired and based on multiple working mechanisms to cooperate at the same time. In the preparation of semiconductor devices, combining semiconductors with certain materials to form Ohmic contact, Schottky contact, or heterojunction is the most common method,[8] which helps to change its internal band structure to achieve different functions. However, most of the current works are in the pursuit of the ultimate Schottky contact or perfect Ohmic contact, ignoring the intermediate states between them. Generally, the pure Schottky contact and perfect Ohmic contact usually require complex preparation procedures, especially combining semiconductor and metal to form a perfect Ohmic contact.[9] Usually, a good Ohmic contact is realized by introducing a heavily doped layer or more elements to improve the electrical conductivity on the surface of the Semiconductor.[10] Such a complicated preparation process is time-consuming and expensive which limits its applicability. Furthermore, the pyro-phototronic effect proposed as a born effect in many non-centrosymmetric semiconductors is used to enhance the performance of photoelectric detection,[11] which should also exist

Y. Zhang, Y.-C. Wang, L. Wang, L. Zhu, Z. L. Wang
CAS Center for Excellence in Nanoscience
Beijing Key Laboratory of Micro-nano Energy and Sensor
Beijing Institute of Nanoenergy and Nanosystems
Chinese Academy of Sciences
Beijing 101400, P. R. China
E-mail: zhulaipan@binn.cas.cn; zlwang@binn.cas.cn

Y. Zhang
Center on Nanoenergy Research
School of Physical Science and Technology
Guangxi University
Nanning 530004, P. R. China

Y.-C. Wang, L. Wang, L. Zhu, Z. L. Wang
School of Nanoscience and Technology
University of Chinese Academy of Sciences
Beijing 100049, P. R. China

Z. L. Wang
School of Material Science and Engineering
Georgia Institute of Technology
Atlanta, GA 30332, USA

The ORCID identification number(s) for the author(s) of this article can be found under https://doi.org/10.1002/adma.202204363.

DOI: 10.1002/adma.202204363

in SiC with a hexagonal crystal structure.[12] While there have been few demonstrations to confirm this so far, which could be attributed to the relatively weak asymmetry in pure SiC single crystals.

In this work, a high-performance PD with potential light mapping and information transition applications based on an n-type N-doped 4H-SiC single crystal chip was fabricated. A notable photoinduced dynamic Schottky effect in the 4H-SiC chip was discovered, which is employed to realize a multifunctional photoelectric sensing. The structure of the 4H-SiC PDs sandwiched between the two reverse "Schottky + Ohmic contact" barriers formed with the elargol (Ag colloid) ensures that both electrodes are in a synergistic state of Ohmic and Schottky modulation, which enables almost tenfold improvement in responsivity compared to that under Ohmic modulation alone. Meanwhile, N-doping can further destroy the symmetry of crystal structure, so that the pyro-phototronic effect becomes non-ignorable, which is conducive to greatly optimizing the response speed and signal strength of the PDs.[13] The 4H-SiC PDs are sensitive to the lightspot coordinate, making the centimeter-scale devices a good candidate for efficient positioning and imaging of the UV light trajectory, so as to achieve possible encrypted transmission of invisible light information.

2. Results and Discussions

2.1. Structure and Basic Performance Characterization

There are four different connection modes between 4H-SiC wafer and electrodes, which are single "Schottky contact", single "Ohmic contact", "Schottky + Ohmic contact" on the same surface, and "Schottky + Ohmic contact" on different surfaces, respectively (as shown in **Figure 1**a). Among them, Schottky contact is to connect the electrode with the smooth surface of 4H-SiC, Ohmic contact is to connect the electrode with the cross section cut by laser, while the combination of the two kinds of connection is to connect the electrode half part to the surface and half part to the cross section cut by laser. Scanning electron microscopy (SEM) images of diamond-knife cutting and laser cutting 4H-SiC cross sections are shown in Figure 1b,c. Obviously, the cross section without laser treatment is smooth and flat but becomes rough surface after laser treatment. Meanwhile, transmission electron microscopy (TEM) diffraction patterns in the lower insets of Figure 1b,c indicates the 4H-SiC crystal structure changed from a well-ordered periodic arrangement to a disordered arrangement after laser treatment, representing the transition from the standard single crystal structure to polycrystal structure within the cross section, which can be also confirmed by TEM images at different magnifications as shown in Figure S1a,b, Supporting Information.[14] The microstructure was also verified by taking the X-ray diffraction (XRD) pattern (shown in Figure 1d) from the horizontally placed smooth 4H-SiC surface (shown in Figure S1c, Supporting Information), and all the characteristic peaks in XRD pattern were in good agreement with the crystal structure of 4H-SiC (the XRD pattern contains not only the characteristic peaks of single crystal SiC but also the polycrystalline characteristic peaks of SiC powder derived from the edge after the laser cutting).[15] The Raman spectra corresponding to the diamond-knife cutting and laser cutting 4H-SiC cross sections were also collected (Figure 1e,f, respectively). All sharp characteristic peaks are found in the diamond-knife cut 4H-SiC sample (Figure 1e) but some of them disappear in laser cut sample

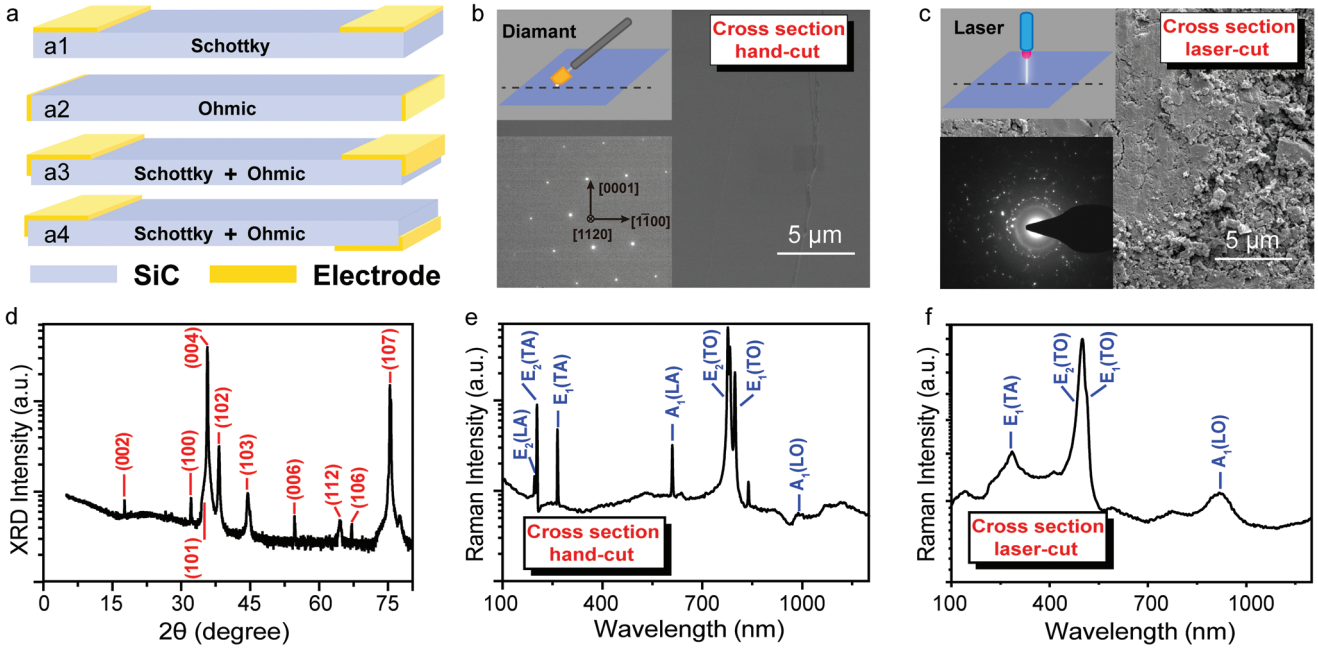

Figure 1. Structure and characterization of the self-powered 4H-SiC PD. a) A schematic of the four electrode connection modes of the 4H-SiC photodetector. b,c) SEM images of diamond-knife-cut and laser-cut cross-sections of 4H-SiC, upper insets: corresponding schematics of cutting methods, lower insets: corresponding TEM diffraction patterns. d) XRD pattern of the 4H-SiC. e,f) Raman spectra of the cross-sections under diamond-knife and laser cutting methods, respectively.

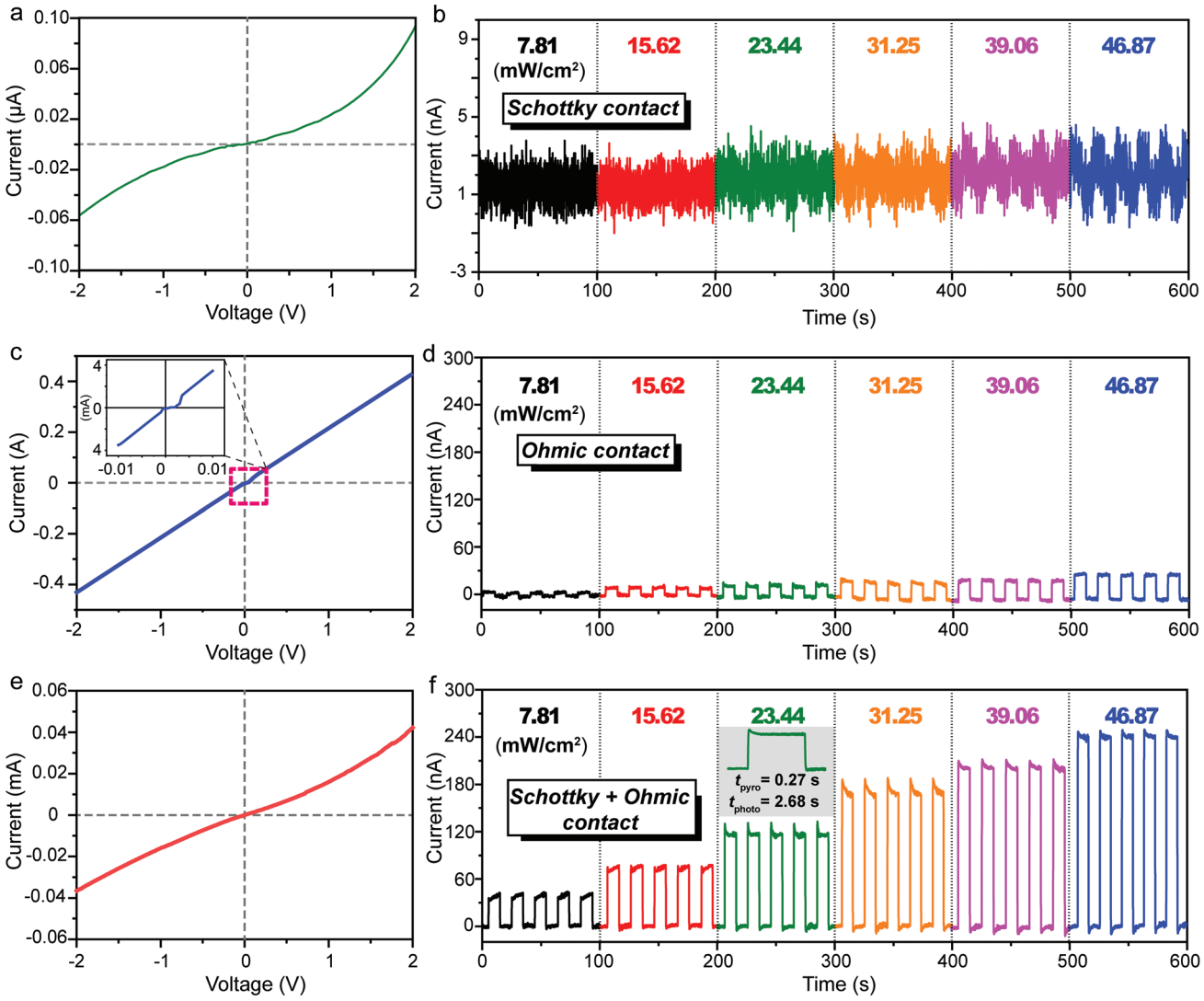

Figure 2. Basic electrical performance of the self-powered 4H-SiC PDs. a) *I–V* curve of a sample with Schottky contact. b) Photoelectric responses of the Schottky contact sample. c) *I–V* curve of a sample with Ohmic contact, insets: magnified view of the step curve at the origin. d) Photoelectric responses of the Ohmic contact sample. e) *I–V* curve of a sample with "Schottky + Ohmic" contact. f) Photoelectric responses of the "Schottky + Ohmic" contact sample. Inset: response signal amplification and response time extraction under the power density of 23.44 mW cm^{-2}.

(Figure 1f). The broadened and asymmetric peaks in Figure 1f indicate that the structure of 4H-SiC undergone laser cutting deviates from the intrinsic standard due to the change of chemical bonds, which is consistent with the literature and the SEM and TEM characterization results above.[16] Moreover, UV–vis spectrum and photoluminescence (PL) spectra (as shown in Figure S1e,f, Supporting Information) were used to estimate the actual band gap width (≈3.2 eV) and the absorption of wavelengths of light (<350 nm) so that the best matching detection range can be found to ensure the detection efficiency.[17]

Basic electrical characteristics of the 4H-SiC PDs with three different connection modes were shown in **Figure 2**. The *I–V* characteristic curve of the 4H-SiC with pure "Schottky contact" is shown in Figure 2a, both the upper and lower parts of the curve show typical rectifying characteristics in opposite directions, indicating that this electrode connection mode forms two reversed Schottky contacts.[18] This means that although this connection mode forms a large internal driving force for carriers, it will form a high energy potential barrier, resulting in a blocked carrier transmission, a disconnected circuit, and difficult signal outputs, which is also reflected in the weak photoelectric responsivity at different light power intensities of a 325 nm laser with a diameter of the laser spot of ≈1 mm (it can be further focused) as shown in Figure 2b (all of the following photoelectric response tests mentioned herein were performed at zero bias voltage). As for the relative pure "Ohmic contact", the *I–V* curve in Figure 2c shows good linear correlation that conforms to Ohm's law, except for the step curve changed at the origin of coordinates, indicating that there exists an emergence of electron tunneling phenomenon.[19] However, such weak signal intensity is not conducive to the detection of the photoelectric signal, as shown in Figure 2d. In general,

Schottky contact tends to create a built-in electric field between materials, which provides a driving force for the external electrons transportation to ensure the smooth current flow in circuits.[20] While the relatively simple "Ohmic contact" will lack the driving force as aforesaid due to less built-in electric field, making the carriers difficult to be transported and collected, so that a high responsivity photodetection will be hardly obtained. To solve this problem, combining the two connection modes ("Schottky + Ohmic contact" as shown in Figure 2e) is a good way to support both the strong driving force and the smooth current transport in the circuit, whose trend of the curve is in the middle state of the two connection modes mentioned above. Due to the support of powerful driving force provided by "Schottky contact", the signal output connected by "Schottky + Ohmic contact" can be improved almost 10 times better than "Ohmic contact" alone (as shown in Figure 2f), thus realizing the optimization in responsivity and efficiency of the PDs.

2.2. Basic Performance of the Self-Powered 4H-SiC PDs

The whole region photoelectric detection was carried out for samples with "Schottky + Ohmic contact" under two kinds of electrode connection (a3: electrodes on the same side, a4: electrodes on the top and bottom sides as shown in Figure 1a). When the electrodes are distributed on both sides, the laser beam starts from the vicinity of the positive electrode and illuminates different positions of the 4H-SiC wafer with a step distance of 1 mm. Each illuminated position will generate a signal, and a 10×10 data array is obtained by collecting the corresponding data of different positions (as shown in Figure S2, Supporting Information). The summary of data points on the corresponding diagonal are plotted in **Figure 3**a (the diagonal data extraction path is shown as the upper left insets of Figure 3a). The data demonstrates that when the laser beam moves from the positive electrode to the negative one, the signal decreases gradually from the positive to zero and then increases gradually in a reversed direction, and the whole 4H-SiC chip conforms to this trend not only from left to right but also from top to bottom as the detailed data shown in Figure S2a, Supporting Information. It is worth noting that when the positive and negative electrodes are located on the upper- and lower-sides of the chip, the peak patterns of the reversed signal are different from that of the positive ones due to the pyro-phototronic effect (magnified reverse signal peaks are shown as the upper right insets of Figure 3a,c, respectively).[11b,21] When the laser irradiates, there exists a rapid response and sharp signal peak in the rising edge of the output positive signal. However, when the signal is reversed, the sharp signal peak at the moment of illumination is replaced by a slowly changing circular peak (all of the corresponding performances expounded below are from samples with "Schottky + Ohmic contact", which are realized by controlling the contact area with different parts of the chip as elaborated in the experimental section). To clarify the reason for the difference in signal peak patterns, the components of the output signal were decomposed, and the possible factors were also studied. The output signal is composed of two parts, one is provided by the pyro-phototronic effect (I_{pyro}), and the other is provided by ordinary photocurrent (I_{photo}).[11a,22] When the laser irradiates on the wafer, the energy carried by the laser will be transferred to the chip with heat instantaneously, the temperature of the area that close to the light source will rise rapidly until higher than the other side, so there will be a crystal tensile along the *c*-axis caused by a certain degree of inflation due to the principle of heat bilging and cold shrinking. Then, the symmetry of materials will be break, thus polarized charges with opposite electrical properties will generate on the upper and lower surfaces because of the noncentral symmetry after laser illumination.[23] As the crystal inflation due to a transient laser illumination, the effective centers of positive and negative charges will be separated from their overlapping original positions to that of what is known as polarized charges. In the transient process, this part of the positive and negative polarized charges will be staggered in opposite directions along the *c*-axis, inducing a current known as an I_{pyro}, which can also be measured in the external circuit to form a current in the same direction as the internal electric field (shown as Figure 3b).[24] Therefore, I_{photo} from photoexcited electron transitions acquisition will be canceled out when I_{pyro} is in the opposite direction, which explains why the spike disappears when the signal is picked up in the opposite direction.

As for the electrodes laid on the same side, the performance of the 4H-SiC self-powered PD in the whole region and the summary of corresponding data points on the diagonal are shown in Figure 3c (the diagonal data extraction path is shown as the upper left insets of Figure 3c) and Figure S3a, Supporting Information, respectively. The pattern of signal change is generally the same as that of the sample with the electrodes on different sides as described above. The only difference is the peak pattern of the negative signals. According to the schematic diagram shown in Figure 3d, the I_{pyro} will remain in the direction up in the 4H-SiC chip, which will lead to an I_{pyro} collected in the same direction as I_{photo} in the external electric circuit when the electrodes are on the same side, so the two signals would reinforce each other rather than cancel out. Then, such sharp and quick response peaks can be detected again just like the forward signal collection. To the best of our knowledge, this is the first demonstration that a pyro-phototronic effect rests in the N-doped 4H-SiC single crystal. By using the pyro-phototronic effect, a fast pyroelectric response time of 0.27 s is achieved, which is almost ten times shorter than that obtained from the steady-state signal (≈2.68 s) under UV illumination. And a maximal transient photoresponsivity of 9.12 nA mW^{-1} (the responsivity extracted when the laser is irradiated near the electrode at a power density of 25 mW) is unveiled with an enhancement of ≈20% relative to the ordinary photoelectric signal (≈7.6 nA mW^{-1}). The test results show regular changes in the row and column, respectively, it is easy to determine the illumination position by data value only in the same row or column, which is of great interest for photoelectric detection and stable light source positioning. But when both rows and columns are taken into consideration or the whole area is detected at the same time, the data values will be repeated, which makes it difficult to clarify the exact illumination area. Noticeably, the direction of current collection will affect the result of signal outputs as abovementioned, hence changing of electrode positions will also produce disparate signals in the same area due to different directions of signal collection, thus providing a new

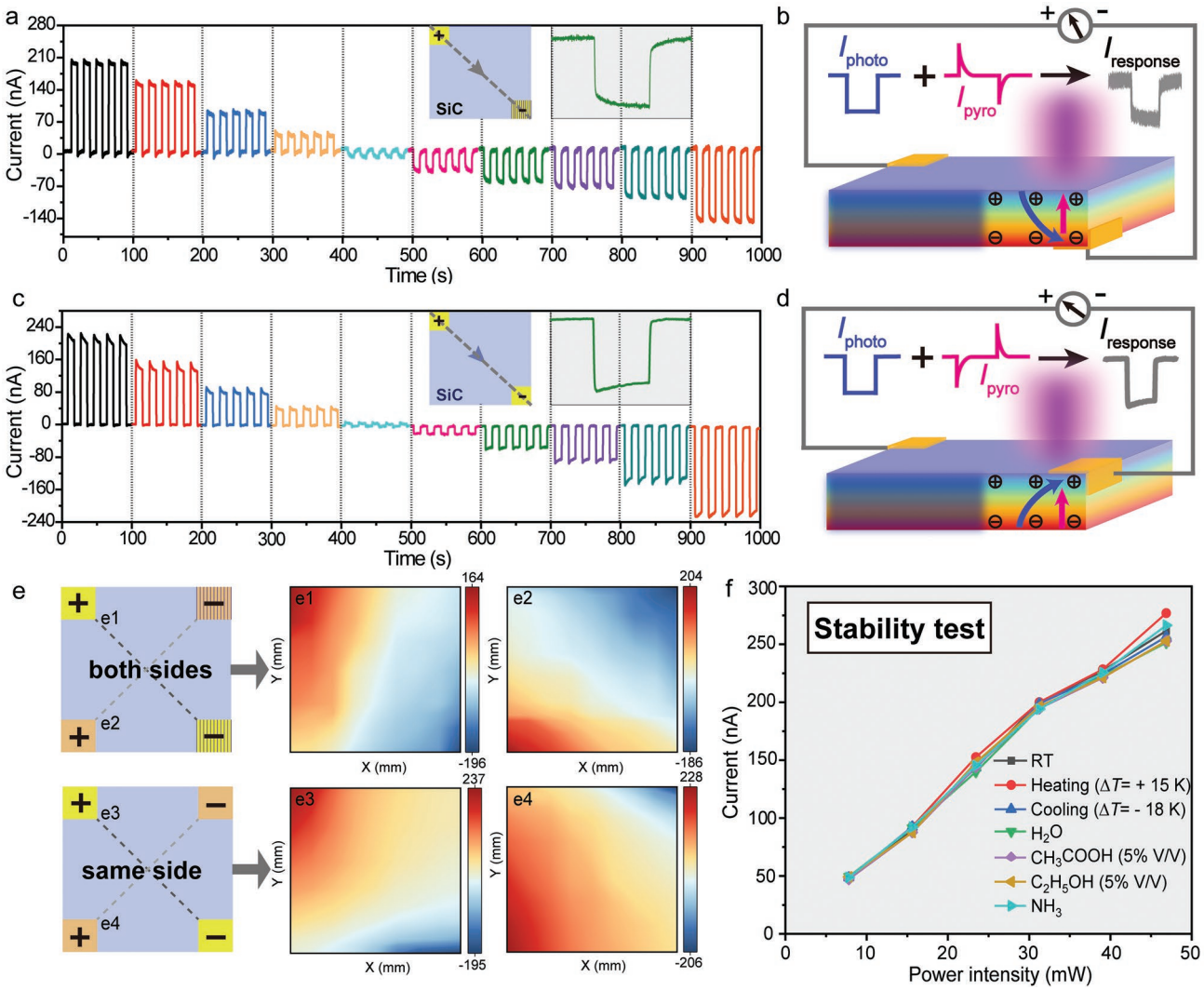

Figure 3. Performance of the self-powered 4H-SiC PD. a) Diagonal data extraction of the whole region photoelectric response of "Schottky + Ohmic" contact with electrodes on different surfaces. Insets: diagonal data extraction path (left), magnified reverse signal peak (right). b) Schematic diagram of the pyro-phototronic effect on the output signal caused by polarized charges generated on different surfaces under illumination. c) Diagonal data extraction of the whole region photoelectric response of "Schottky + Ohmic" contact with electrodes on the same surface. Insets: diagonal data extraction path (left), magnified reverse signal peak (right). d) Schematic diagram of the pyro-phototronic effect on the output signal caused by polarized charges generated on the same surface. e) The current intensity diagram of the whole region produced by the two groups of electrodes with different distribution modes. f) Schematic diagram of stability tests at different temperatures and atmospheres.

idea to solve the problem of data duplication. As expected, the full-area response performances of the two electrode distribution modes both changed when the original "upper left + lower right" electrode combination is replaced by "upper right + lower left" as shown in Figures S2b,3b, Supporting Information, respectively. Based on these findings, the four electrodes can be divided into "upper left + lower right" and "upper right + lower left" two groups, then connected to two sets of signal receiver separately. The same location of the chip will generate two different signals, and the two different data values corresponding to the same position can be combined to form the coordinate to represent this irradiated position, that is, the data points corresponding to the same position in Figure S2a,b, Supporting Information are combined, as well as the data points corresponding to the same position in Figure S3a,b, Supporting Information are combined. The response diagram after combination is shown in Figure 3e (e1 and e2: electrodes on upper and lower surfaces; e3 and e4: electrodes on the same surface), where e1 and e3 correspond to the "upper left + lower right" combination, e2 and e4 correspond to the "upper right + lower left" combination. The response law of electrodes on the same surface or both surfaces is basically consistent, and the arrangement and combination of the two groups of electrodes at different positions on the same chip can get rid of data repetition and realize unique positioning of light irradiation. Additionally, to ensure the stable use of the device in practice, it is necessary to test the stability in different environments. The output currents of samples under different temperatures, atmospheres, and acid–base simulation environments are tested (Figure 3f and Figure S4, Supporting Information). The current versus

power intensity plots exhibit negligible deviation in response to different environments, showing good stability of the device. Such results support the newly proposed device to be used in practical applications.

2.3. Applications of the Self-Powered 4H-SiC PDs

Through the study of the basic photoelectric response of the 4H-SiC wafer, it is found that different connection modes and structural design will cause extraordinary differences, and the ingenious arrangement and combination of the results will be of great significance in practical applications. As the unique signal combination will be generated when the laser irradiates on different positions of the chip, it is easy to locate and track the incident laser, especially to overcome the disadvantage of high energy ultraviolet light without visible trace in moving process. For example, when a laser moves in a zigzag pattern on a chip, two sets of electrodes should be separately connected to two series of signal receivers at first, and then the irradiated areas on the chip will generate responding electrical signals by turn. The first set of data values will be generated as the electrodes connected in the way shown in the insets of **Figure 4**a, and the second set of data values will be generated as the electrodes connected in the way shown in the insets of Figure 4c. As two sets of data points acquired, the full-area data representation diagram obtained under the two electrode combination modes will realize the effects as shown in Figure 4b,d, respectively (the imaging pictures shown in Figure 4b,d can be obtained by coupling the two groups of data from the two sets of electrodes under different combination modes, which cannot be obtained by single Group 1 or 2). It means that the path of laser movement can be easily obtained by comparing the two sets of electrical signals collected from the 4H-SiC chip with the data map of the whole region measured in front, thus achieving both positioning and imaging functions at the same time.

As a result, more applications can be exploited based on this performance as shown in Figure 4e, including precise light-path adjustment for dedicated optical instruments and encrypted information transmission. In the process of adjusting the path with laser emitting invisible light, it is difficult to provide reference for the accurate adjustment of incidence and azimuth angles because of the undetermined light spot position. However, if the photodetector chip is added in the path, the spot position and moving path will become visible to guide the direction adjusting thus improves working efficiency. Besides, except for the basic laser writing imaging, it also reveals great potential in the field of information communication, especially the encryption communication, due to fast signal conversion rather than complex multi-channel information processing.[25] Both the conventional acoustic wave and electromagnetic wave are easily intercepted during the process of information transmission, while the application of this self-powered 4H-SiC PD can provide a new design idea for encryption transmission to a certain extent. Because light wave possesses high propagation flexibility and invisible light itself is difficult to be found and captured, which provides a good environment for signal encryption. In addition, the information of the signal generated on the surface of the chip can be customized. The whole detector can generate different signals, which can be endowed with a variety of practical meanings. At the same time, the encryption mode can be updated flexibly by changing the position and combination of electrodes. Even if the light wave can be captured, the actual meaning of the light wave cannot be cracked, which provides a powerful guarantee for the secret transmission of information. Moreover, the lightweight and simple structure with flexible size and self-powered characteristics within the chip brings more advantages for the practical applications, supporting the device to possess more possibilities for a wider application in many scenarios.

2.4. Working Mechanism of the Self-Powered 4H-SiC PDs

The excellent performance and application potentials demonstrated above are attributed to a photoinduced dynamic Schottky effect within the heterostructure formed by the single crystal 4H-SiC and the metal electrodes. Photoinduced dynamic Schottky effect is a dynamic reversible process in which the Schottky barrier formed between metal and semiconductor materials will be changed under a light illumination and return to its original state with the removal of illumination. This photoinduced dynamic Schottky effect enables a high responsivity self-powered photoelectric detection of conventional third-generation semiconductor 4H-SiC with the simplest fabrication process and the most lightweight structure design. The effect is achieved by sandwiching a 4H-SiC wafer between two reversed Schottky barriers that fused with Ohmic contacts, using the potential difference brought by light-induced band structure elevation and built-in electric field constructed by Schottky contact,[26] which provides a driving force for the electrons flow. In addition, the advantage of small resistance brought by Ohmic contact would largely weaken the obstruction of electrons in the circulation process, so that the responsivity could be enhanced almost tenfold. Meanwhile, this effect is based on the interaction of distinct types of heterojunctions formed when the semiconductor contacts with the metal, so the energy band theory is needed to clarify the working mechanism involved in the operation of the device. In the process of photoinduced dynamic Schottky effect, it is inevitable to bring the difference of heights of the two Schottky barriers, which is caused by the unbalanced scattering energy generated by illumination at different chip positions, as shown in **Figure 5**a1. As the light gets closer to the one electrode, the Schottky barrier formed on the closer electrode side will be greatly raised and higher than that on the other electrode side, which will determine the strength and direction of the final electric current, as shown in Figure 5a2. As shown in Figure 5a3, when there is no light excitation, there will be no photoinduced carriers in the energy band and hence no photocurrent.[27] When the chip with "Schottky + Ohmic contact" is irradiated by a 325 nm laser, the band structure formed at the irradiated end will increase with the elevation of the metal and 4H-SiC work functions excited by light,[26] while the band structure will return to the initial state again after the light off. For example, when laser irradiates on the side near the positive electrode, where 4H-SiC wafer and metal electrode connected under the "Schottky + Ohmic contact" mode, the band structure near the positive side will be deflected upward, and then the Schottky barrier will be raised and higher than the band

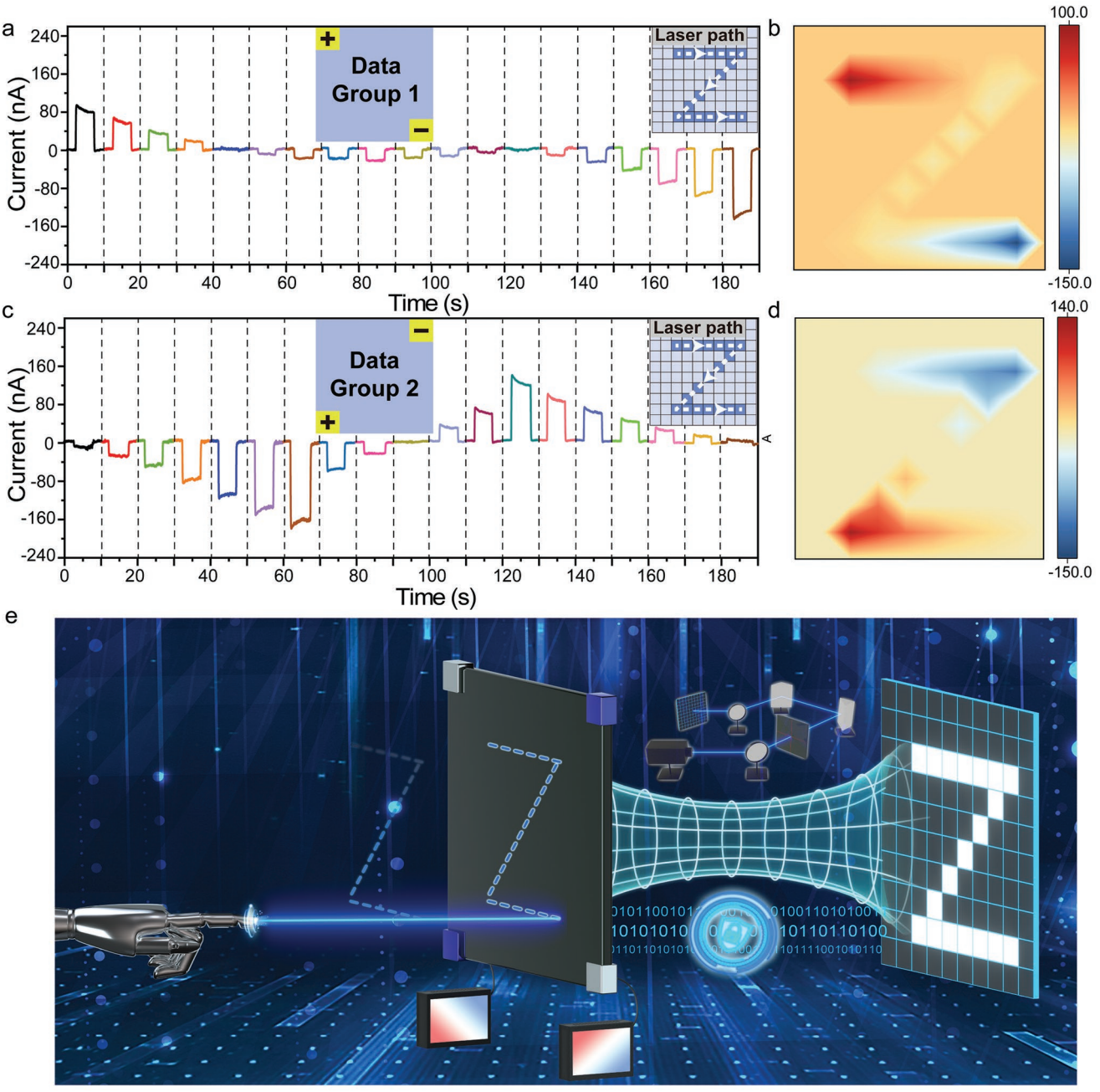

Figure 4. Applications of the self-powered 4H-SiC PD. a) The photoelectric response generated by the combination of upper left and lower right electrodes during application. Insets: Electrode position distribution corresponding to Group 1 (left), and the moving path of illumination (right). b) A mapping image of the optical path formed by laser movement under electrode combination Group 1. c) The photoelectric response generated by the combination of upper right and lower left electrodes during application. Insets: Electrode position distribution corresponding to Group 2 (left), and the moving path of illumination (right). d) A mapping image of the optical path formed by laser movement under electrode combination Group 2. e) A Schematic of operation and application scenario of the device.

structure near the negative side. Thus, the photo-excited electrons are driven to transport between the two counterbalanced Schottky barriers. The same is true when the light is near the negative electrode, except that the electrons move in the opposite direction as shown in Figure 5a3. However, with the similar structure and principle, the other two modes electrode connection (pure "Schottky contact" and main "Ohmic contact") cannot achieve the same effect, the reason behind it is worth for in-depth analysis. In a mode where the metal electrodes are connected to the 4H-SiC wafer surface in pure "Schottky contact", forming strong Schottky contact between the two materials, a strong built-in electric field will be formed at the contact interface.[28] Although it can provide a greater driving force for the movement of photoinduced electrons other than the energy brought by the

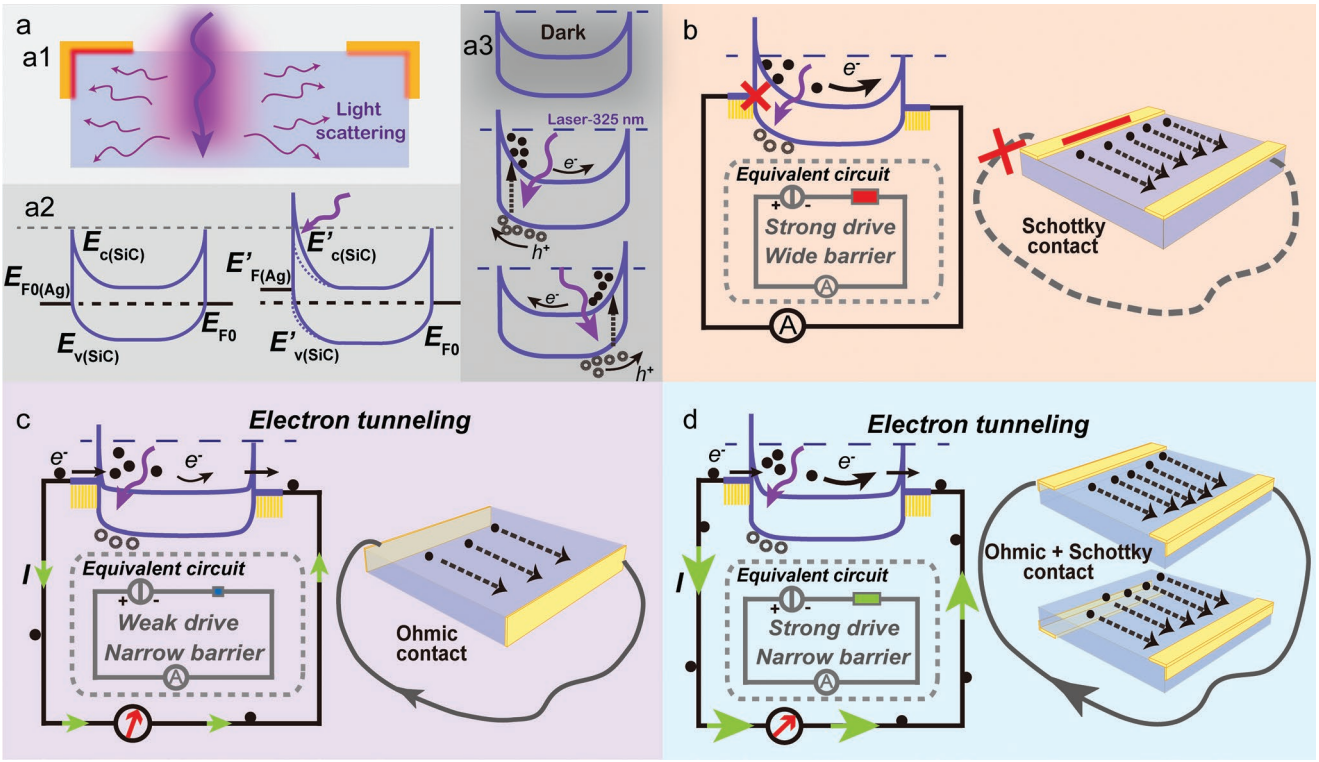

Figure 5. Working mechanism of the self-powered 4H-SiC PD. a) Energy band variation of "Schottky + Ohmic" contact under different illumination conditions. a1) Diagram of laser scattering in SiC crystal; a2) schematic diagram of energy band change after illumination; a3) schematic diagram of energy band changes corresponding to illumination at different positions. b–d) The energy band changes of the self-powered 4H-SiC PD and equivalent schematics under Schottky contact (b), Ohmic contact (c), and "Schottky + Ohmic" contact (d), respectively.

band elevation, it would also be a hindrance because of the built-in electric fields in the opposite direction on both sides, that is, electrons consume a lot of energy in the process of transmission caused by the reversed wide barrier. It is a big chance that there is not enough driving force to ensure the photoinduced electrons jumping over the high and wide left barrier and then recombine with the trapped holes in the left of the valence band to complete the circuit circulation, as shown in Figure 5b. Equivalent circuit diagram is shown in the illustrations of Figure 5b, powerful built-in electric field generated by the Schottky contact on the electron movement direction can be regarded as strong driving power, and the one in the opposite direction is just like a huge resistance of the motion of the electrons. In the process of electron transport, the energy provided by the extra lifted energy band is far from enough to ensure the electrons jumping over the left Schottky barrier. In a sense, the circuit can be considered as disconnected in this case.

When the metal is connected only to the laser-cut 4H-SiC cross section, the connection is formed mainly by Ohmic contact. In this kind of device fabrication, a large number of surface states will be introduced into the cutting surface of the semiconductor due to the instant release of high energy and heat during the laser cutting process, whose effect is similar to the complex process of heavy doping treatment.[26] In this case, it shows obvious features of the Ohmic contact, representing no large built-in electric field on the border within the material, which also means no strong driving force and no big reverse obstacles as shown in Figure 5c. Electrons can shuttle at the interface, and even accompanied by electron tunneling occurrence due to the narrow barrier, which is also confirmed by the previous *I–V* curve in Figure 2c. According to the circuit diagram, it can be found that even if the barrier is negligible, the weak driving force will only result in a tiny photoelectric current. A similar effect can also be verified in monocrystal silicon (Si). Compared with the n-type N-doped 4H-SiC, there is a lack of strong light scattering within Si single crystal, which is difficult to form an asymmetric Schottcky barriers. Therefore, response signals can only be generated near the edge of the electrodes when the photoinduced dynamic Schottky effect occurs, as shown in Figure S5a, Supporting Information. In the region away from the electrodes, the optoelectronic signal output cannot be completed due to the lack of unbalanced Schottky barriers and hence leading to a weak driving force of carriers, which will result in poor responsivity and low efficiency of the Si single crystal PD, as shown in Figure S5b,c, Supporting Information. Consequently, the photoinduced dynamic Schottky effect inside 4H-SiC is demonstrated to be much more sensitive to the illumination of UV light, and more favorable internal conditions for photoexcited electron transport.

If the two connection modes mentioned above can be skillfully combined and the effect can be controlled in the middle state of Ohmic and Schottky modulation, the disadvantages of each other could be overcome, which has not only sufficient driving force but also little barrier to ensure the electrons fluently flowing and transporting in the whole current pathway

as shown in Figure 5d. The realization of this connection state requires the metal electrodes to satisfy Schottky contact with the 4H-SiC wafer surface and Ohmic contact with the laser-treated cross-section simultaneously, and the proportion of different connection modes can be regulated by the contact area, as shown in Figure 5d. In this state, whether the electrodes are in the same plane or both on the upper and lower surfaces will not affect the great increase in signal output. When the illumination is near the positive electrode, the band of this side will be raised and the photoexcited electrons will flow along the direction from high to low, forming a closed loop. On the other hand, when light near the negative electrode, the band of the side near the negative electrode will be raised again, while the band of the positive side will turn back to the initial state, lower than the band near the negative side. Then, the electrons will transport in the same way from high to low. The current flows reversely and form a closed loop opposite to the front direction, which also explains the phenomenon that why the output signal will be reversed as the change of light spot positions. This mechanism is also applicable to other semiconductor structures with different depths of potential barrier formed within the material, and the limited area with photoelectric effect will be different to some extent based on the number of freely moving electrons and the strength of the junction.

3. Conclusions

Based on the n-type N-doped 4H-SiC single crystal, high-performance self-powered UV PDs with great application prospect were fabricated using a photoinduced dynamic Schottky effect and the pyro-phototronic effect within the 4H-SiC wafer. Above all, a co-modulation of Schottky and Ohmic contacts via delicate position designs of Ag electrodes after a laser-cutting treatment of the 4H-SiC chip is employed to realize the PDs. Moreover, the pyro-phototronic effect induced by instantaneous UV illumination is demonstrated in the N-doped 4H-SiC, which brings great enhancement of both response speed (increased to ten times) and the maximal transient photoresponsivity (increased by 20%) compared to the steady-state photoelectric signal. Under UV illumination, the balance of the two co-modulated Schottky barriers is broken dynamically with the light horizontally moving in the two-dimensional plane parallel to the centimeter-scale chip, resulting in a distinct current corresponding to different light spot position. Based on this mechanism, a self-powered UV PD is demonstrated with simply fabrication processes and is believed to possess high potential in positioning and encrypted information transmission applications. In addition, the working mechanisms of the photoinduced dynamic Schottky effect elaborated for "Schottky + Ohmic contact" involved in the device are of great significance to the development of both basic physics and practical applications in this vital third-generation semiconductor.

4. Experimental Section

Device Fabrication: The commercially available 4H-SiC crystal chips grown by physical vapor transport (PVT) method with a nitrogen doping level of $>10^{18}$ cm^{-3} and 350 ± 10 µm in thickness (purchased from Helios New Materials Ltd.) were first cut into the expected size with a laser cutting machine. Thin copper wires were then connected to the chips to make electrodes using silver glue, which can be dried at room temperature and dispersed in an alcohol solution. A Schottky contact will be formed if the copper wire is only connected to the upper or lower surface, and an Ohmic contact will be formed if the copper wire is only connected to laser-cutting cross sections of the wafer. Therefore, a "Schottky + Ohmic contact" was formed when copper wires were simultaneously connected to both the surface and cross sections of the chip. The area covered by electrodes at different positions on the chip will determine the strength of different contact effects, which can be adjusted by flexible masks with different sizes and can also be estimated by measuring the resistance. In this work, the electrodes were respectively distributed near the diagonal vertex of the chip (as shown in Figure S6a, Supporting Information), but the electrode positions can be arbitrarily distributed according to the actual needs, and the distance between the electrodes was also not fixed.

Characterization: The microstructure and morphology of samples were characterized using a field emission scanning electron microscope (SU8020, Japan). The diffraction patterns and atomic arrangements were characterized by a transmission electron microscope (Tecnai G20, USA). The photoluminescence (PL) and Raman spectra were acquired using the spectrometer (LabRAM HR Evolution, France) with an inflammation laser (Raman: wavelength 532 nm, PL: wavelength 325 nm). Transmission spectra were acquired by an ultraviolet–visible spectrophotometer (UV-3600, Japan). The samples were baked with silver electrode at room temperature for 30 min to test the electrical properties. The X-ray diffraction patterns of the samples were recorded with an X-ray diffractometer (XRD, XPert3 Powder, The Netherlands). The optical input stimuli were provided by a He–Cd dual-color laser (wavelength 325 nm, Model No. IK3501R-G, Kimmon Koha Co, Ltd, Japan). A continuously variable filter was used to control the light power density, which was measured with a thermopile powermeter. *I–V* characteristics of the device were measured and recorded with a self-developed, computer-controlled measurement system with Stanford SRS Low-noise current preamplifier (SR560)/precision point measurement system (DS345) in connection with a data collector (BNC-2120) as shown in Figure S6b, Supporting Information.

Statistical Analysis: All structural characterization data and electrical performance data were exhibited without the use of transformation, standardization, evaluation of outliers, or other pre-processing means. Due to inevitable systematic errors, the thickness test of the sample may have an error value in the range of 10 µm, and the data was presented as 350 ± 10 µm. Under the seven testing environments as shown in Figure 3f, each extraction of the response irradiated by the laser at the same position with different power densities was the average result of five separately samplings (n = 5), and the detailed testing information is given in the legends. The response signals obtained under different illumination intensity and the response at different positions of the chip were both the results of five periodic samplings.

Supporting Information

Supporting Information is available from the Wiley Online Library or from the author.

Acknowledgements

This research was supported by the National Natural Science Foundation of China (Grant No. 52192610 and 52192613) and the National Key R&D Project from Minister of Science and Technology (2021YFA1201601).

Conflict of Interest

The authors declare no conflict of interest.

Data Availability Statement

The data that support the findings of this study are available from the corresponding author upon reasonable request.

Keywords

photoinduced dynamic Schottky effect, pyro-phototronic effect, self-powered devices, sensors, SiC

Received: May 14, 2022
Revised: July 3, 2022
Published online:

[1] a) D. Nakamura, I. Gunjishima, S. Yamaguchi, T. Ito, A. Okamoto, H. Kondo, S. Onda, K. Takatori, *Nature* **2004**, *430*, 1009; b) K. Watanabe, T. Taniguchi, H. Kanda, *Nat. Mater.* **2004**, *3*, 404.

[2] J. Hicks, A. Tejeda, A. Taleb-Ibrahimi, M. S. Nevius, F. Wang, K. Shepperd, J. Palmer, F. Bertran, P. Le Fèvre, J. Kunc, W. A. de Heer, C. Berger, E. H. Conrad, *Nat. Phys.* **2013**, *9*, 49.

[3] a) H. Morkoç, S. Strite, G. B. Gao, M. E. Lin, B. Sverdlov, M. Burns, *J. Appl. Phys.* **1994**, *76*, 1363; b) E. Bekaroglu, M. Topsakal, S. Cahangirov, S. Ciraci, *Phys. Rev. B.* **2010**, *81*, 075433.

[4] a) X. Qian, P. Jiang, R. Yang, *Mater. Today Phys.* **2017**, *3*, 70; b) P. G. J. Millán, X. Perpiñà, A. Pérez-Tomás, J. Rebollo, *IEEE Trans. Power Electron.* **2014**, *29*, 2155; c) N. G. Wright, A. B. Horsfall, *J. Phys. D. Appl. Phys.* **2007**, *40*, 6345.

[5] a) Y. Feng, Xiaobin, S. Aslam, Z. Yuegang, D. Franz, J. H. Zhao, M. Weiner, *IEEE J. Quantum Electron.* **2004**, *40*, 1315; b) R. Hillenbrand, T. Taubner, F. Keilmann, *Nature* **2002**, *418*, 159.

[6] a) J. B. Casady, R. W. Johnson, *Solid-State Electron.* **1996**, *39*, 1409; b) Y. Peng, J. Lu, X. Wang, W. Ma, M. Que, Q. Chen, F. Li, X. Liu, W. Gao, C. Pan, *Nano Energy* **2022**, *94*, 106945; c) S. Shahzad, S. Javed, M. Usman, *Front. Mater.* **2021**, *8*, 613825.

[7] a) S. Xu, Y. Qin, C. Xu, Y. Wei, R. Yang, Z. L. Wang, *Nat. Nanotechnol.* **2010**, *5*, 366; b) Z. L. Wang, *Adv. Mater.* **2012**, *24*, 280; c) W. Tian, Y. Wang, L. Chen, L. Li, *Small* **2017**, *13*, 1701848.

[8] a) F. Hossein-Babaei, M. Gharesi, M. Moalaghi, *ACS Appl. Mater. Interfaces* **2017**, *9*, 26637; b) S. Abbas, M. Kumar, H. S. Kim, J. Kim, J. H. Lee, *ACS Appl. Mater. Interfaces* **2018**, *10*, 14292.

[9] M. Spera, G. Greco, D. Corso, S. Di Franco, A. Severino, A. A. Messina, F. Giannazzo, F. Roccaforte, *Materials* **2019**, *12*, 3468.

[10] a) S. Rascunà, P. Badalà, C. Tringali, C. Bongiorno, E. Smecca, A. Alberti, S. Di Franco, F. Giannazzo, G. Greco, F. Roccaforte, M. Saggio, *Mater. Sci. Semicond. Process.* **2019**, *97*, 62; b) M. Spera, G. Greco, R. Lo Nigro, C. Bongiorno, F. Giannazzo, M. Zielinski, F. La Via, F. Roccaforte, *Mater. Sci. Semicond. Process.* **2019**, *93*, 295.

[11] a) Z. Wang, R. Yu, C. Pan, Z. Li, J. Yang, F. Yi, Z. L. Wang, *Nat. Commun.* **2015**, *6*, 8401; b) Z. Wang, R. Yu, X. Wang, W. Wu, Z. L. Wang, *Adv. Mater.* **2016**, *28*, 6880.

[12] K. E. Prasad, K. T. Ramesh, *J. Alloys Compd.* **2019**, *770*, 158.

[13] Y. Wang, L. Zhu, Y. Feng, Z. Wang, Z. L. Wang, *Adv. Funct. Mater.* **2018**, *29*, 180711.

[14] T. Okada, H. Kawahara, Y. Ishida, R. Kumai, T. Tomita, S. Matsuo, S. Hashimoto, M. Kawamoto, Y. Makita, M. Yamaguchi, *Appl. Phys. A* **2008**, *92*, 665.

[15] M. Wilhelm, F. Kubel, W. Wruss, *Powder Diffr.* **2001**, *16*, 42.

[16] L. Wan, D. Zhao, F. Wang, G. Xu, T. Lin, C.-C. Tin, Z. Feng, Z. C. Feng, *Opt. Mater. Express* **2017**, *8*, 119.

[17] a) T. Ryan, J. Hennessy, C. Harrison, S. Y. Wang, G. Webster, A. Majima, *Mater. Sci. Forum* **2007**, *556–557*, 299; b) A. L. Beck, X. Guo, H. D. Liu, A. Ghatak-roy, J. C. Campbell, *Proc. SPIE* **2006**, *6372*, 63720O.

[18] Y. Shen, M. Wan, *Synth. Met.* **1998**, *98*, 147.

[19] a) T. Fujisawa, T. Hayashi, Y. Hirayama, H. D. Cheong, Y. H. Jeong, *Appl. Phys. Lett.* **2004**, *84*, 2343; b) R. A. Kraya, L. Y. Kraya, *J. Appl. Phys.* **2012**, *111*, 064302.

[20] X. Tang, S. Wang, Y. Liang, D. Bai, J. Xu, Y. Wang, C. Chen, X. Liu, S. Wu, Y. Wen, D. Jiang, Z. Zhang, *Phys. Chem. Chem. Phys.* **2022**, *24*, 7323.

[21] Y. Zhang, J. Chen, L. Zhu, Z. L. Wang, *Nano Lett.* **2021**, *21*, 8808.

[22] H. Zou, G. Dai, A. C. Wang, X. Li, S. L. Zhang, W. Ding, L. Zhang, Y. Zhang, Z. L. Wang, *Adv. Mater.* **2020**, *32*, 1907249.

[23] W. Peng, X. Wang, R. Yu, Y. Dai, H. Zou, A. C. Wang, Y. He, Z. L. Wang, *Adv. Mater.* **2017**, *29*, 1606698.

[24] H. Zou, C. Zhang, H. Xue, Z. Wu, Z. L. Wang, *ACS Nano* **2019**, *13*, 12259.

[25] J. Han, J. Jiang, T. Wu, Y. Gao, Y. Gao, *Nanomaterials.* **2022**, *12*, 289.

[26] S. K. Ravi, W. Sun, D. K. Nandakumar, Y. Zhang, S. C. Tan, *Sci. Adv.* **2018**, *4*, eaao6050.

[27] J. Zheng, H. Chong, L. Wang, S. Chen, W. Yang, G. Wei, F. Gao, *J. Mater. Chem. C* **2020**, *8*, 6072.

[28] A. Gali, D. Heringer, P. Deák, Z. Hajnal, T. Frauenheim, R. P. Devaty, W. J. Choyke, *Phys. Rev. B* **2002**, *66*, 125208.